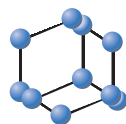


RESEARCH ARTICLE


**BENTHAM
SCIENCE**

Engineering and Characterization of Smart Material in Real-Time Mode



Jagadeesh Suriyaprakash^{a,b}, Xiu L. Ma^{a,c,*}, Yin L. Zhu^a, Yu J. Wang^a, Xiao B. Hu^a, Min J. Zou^{a,b} and Yan P. Feng^{a,b}

^aShenyang National Laboratory for Materials Science, Institute of Metal Research, Chinese Academy of Sciences, 72 Wenhua Road, Shenyang 110016, China; ^bUniversity of Chinese Academy of Sciences, Beijing 100039, China; ^cState Key Laboratory of Advanced Processing and Recycling of Non-ferrous Metals, Lanzhou University of Technology, Lanzhou 730050, China

Abstract: Background: Bismuth titanate ($\text{Bi}_4\text{Ti}_3\text{O}_{12}$) is one of the prominent candidates in lead free ferroelectric/piezoelectric materials and also in photocatalytic materials. Moreover, it is mainly utilized in the piezotronic-smart material field. $\text{Bi}_4\text{Ti}_3\text{O}_{12}$ demands more efforts to enhance its functional properties by modifying its chemical as well as physical features. Currently, the new class of materials is required to fulfill the necessity of multi-functionality with better performance. In this context, we proposed a novel model material and fabricated it in a facile way.

Methods: In this report, we present a one-step route to synthesizing and studying of the smart material $x\text{Bi}-\text{Bi}_{4-x}\text{Ti}_3\text{O}_{12-y}-\text{Bi}_4\text{Ti}_3\text{O}_{12}$ at real-time mode in High Resolution Transmission Electron Microscope (HRTEM) at micro-scale level.

Results: $\text{Bi}_4\text{Ti}_3\text{O}_{12}$ shows significant changes under e-beam, which is converted into Bi metal nanocrystals decorated on the non-stoichiometric A-site deficient $\text{Bi}_{4-x}\text{Ti}_3\text{O}_{12-y}$ microparticle. The surface and electronic characteristics study demonstrates the presence of Bi and also divulges that there is a modification in electronic band structures. The Fermi levels of the non-irradiated and irradiated $\text{Bi}_4\text{Ti}_3\text{O}_{12}$ were found to be 1.45 ± 0.1 eV and 1.8 ± 0.1 eV above the valence band maximum, respectively. The chemical composition analysis of the resultant material shows signs of the existence of $x\text{Bi}-\text{Bi}_{4-x}\text{Ti}_3\text{O}_{12-y}-\text{Bi}_4\text{Ti}_3\text{O}_{12}$.

Conclusion: A new class of multifunctional material like metal-n-type semiconductor / ferroelectric ($x\text{Bi}-\text{Bi}_{4-x}\text{Ti}_3\text{O}_{12-y}-\text{Bi}_4\text{Ti}_3\text{O}_{12}$) is synthesized at a micro-scale level in HRTEM and investigated systematically. The formation of the novel structure may follow the Knotek-Feibelman mechanism involving the Auger decay of oxygen and local bond-breaking phenomenon in Aurivillius phase double layered perovskite $\text{Bi}_4\text{Ti}_3\text{O}_{12}$.

Keywords: Band engineering, $\text{Bi}_4\text{Ti}_3\text{O}_{12}$, electronic structure, ferroelectric, functional material, transmission electron microscopy, x-ray photoelectron spectroscopy.

1. INTRODUCTION

In the quest for the novel multifunctional materials (which have properties, scientists can manipulate); smart materials are the prominent candidates. Smart materials contain one or more properties that can be extensively altered in a controlled manner by external stimuli, such as stress, temperature, moisture, electric or magnetic fields, etc. [1, 2]. Ample of research has been focused on metals, ceramics, polymers, nanocomposites, biomaterials to engineer the

smart materials from the last two decades achieved by the modification of materials (structure, shape, composition, defects, etc.) [3-5]. Among the electronic smart materials, piezo and ferroic materials have been extensively studied because of their broad application in electrical and electronic industries [6-8]. Despite the fact that various new materials have been explored and investigated till now; there is still space for engineering the novel smart materials. Nowadays, most of the researchers are being focused on the commercialization of technologically important functional materials (e.g. Miniaturization of the device through low-cost fabrication technique at nano-scale precision). Electron beam (e-beam) is a very promising technique in the device as well as nanostructured fabrication [9]. It is primarily used in the

*Address correspondence to this author at the Shenyang National Laboratory for Materials Science, Institute of Metal Research, Chinese Academy of Sciences, 72 Wenhua Road, Shenyang 110016, China; Tel: +86-024-2397 1845; E-mail: xlma@imr.ac.cn

fabrication of electro-ceramic devices which are around ten nanometer scales rather than conventional device fabrication techniques. Today, most of the electronic devices are highly densified packages. For this purpose, e-beam technique becomes more attractive since the e-beam can be easily focused on the desired area on a nanometer scale using precisely controlled magnetic lenses. Our previous study illustrated that one can design the metallic nanocrystals supported in non-stoichiometric perovskite material, while its counterpart is exposed under e-beam [10]. Furthermore, to step-up this innovative technique, we fabricate the novel smart material ($x\text{Bi}-\text{Bi}_{4-x}\text{Ti}_3\text{O}_{12-y}-\text{Bi}_4\text{Ti}_3\text{O}_{12}$) as like as metal-n-type semiconductor- piezo/ferroelectric at the micro-scale from nano-scale level. In the search for a new class of materials, we compose a model which is the combination of semimetal / high magnetoresistance and piezo-ferroelectric / multiferroic properties as shown in Fig. (1). To achieve this proposed model, we choose bismuth (Bi) and bismuth titanate ($\text{Bi}_4\text{Ti}_3\text{O}_{12}$; BTO) as prototype materials.

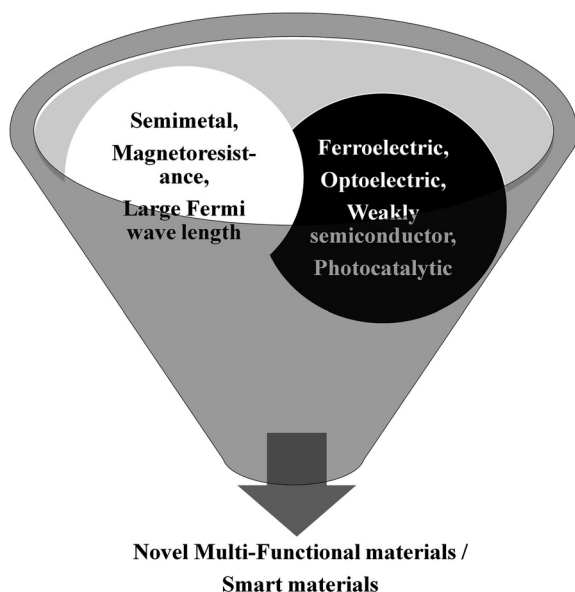


Fig. (1). A schematic model for obtaining the novel smart materials.

Bi possesses a set of peculiar properties (semimetal, high magnetoresistance and high Fermi wavelength) [11, 12]. Moreover, Bi will show a semimetal to semiconductor transition due to quantum confinement effect and enhanced thermoelectric properties at the nanoscale [13, 14]. These properties make the Bi able to be utilized in electronic, optical and phononic applications. BTO is an extensively studied piezo/ferroelectric material, which has a layered pseudo perovskite-like structure. It can be considered an orthorhombic structure with $a = 5.410 \text{ \AA}$, $b = 5.448 \text{ \AA}$ and $c = 32.83 \text{ \AA}$ [15-17]. The BTO has a high Curie temperature (675°C) and exhibits high polarization along a -axis ($50\mu\text{C}/\text{cm}^2$) which makes it a good candidate for high-temperature memory devices [18]. In addition, as a lead free ferroelectric material, it sustains a wide area of applications ranging from capacitors to non-volatile memory devices, including various types of sensors and photocatalyst [19, 20]. Besides, void A-site cation deficient perovskite materials

show unique features [21, 22]. In this report, we investigated the smart material, which consists of semimetal Bi, piezo/ferroelectric BTO and A-site cation deficient $\text{Bi}_{4-x}\text{Ti}_3\text{O}_{12-y}$ at real-time mode in High Resolution Transmission Electron Microscope (HRTEM) at ambient temperature. We employed the X-ray photoelectron spectroscopy method to evaluate the electronic properties as well as the surface ones along with the HRTEM technique.

2. MATERIALS AND METHODS

2.1. Synthesize of BTO Microparticles

The BTO microparticles were synthesized by sol-gel method. The precursors used for preparing BTO sol were bismuth nitrate pentahydrate [$\text{Bi}(\text{NO}_3)_3 \cdot 5\text{H}_2\text{O}$], and titanium IV butoxide [$\text{Ti}(\text{OCH}_2\text{CH}_2\text{CH}_2\text{CH}_3)_4$]. Acetic acid [CH_3COOH] and acetylacetonate [$\text{C}_5\text{H}_8\text{O}_2$] utilized as a solvent and a chelating ligand, respectively. All chemicals are purchased from Sinopharm chemical reagent Co.Ltd, China as AR grade. The Bi^{3+} solution is prepared by dissolving 50 mM of $\text{Bi}(\text{NO}_3)_3 \cdot 5\text{H}_2\text{O}$ in the 15 ml of acetic acid. The solution is heated and stirred for 25 min. Then 5 ml of equal molar acetylacetonate was added to it. Finally, titanium butoxide in the stoichiometric ratio is slowly added to the solution with continuous stirring for 25 min to prepare BTO sol. The BTO sol has dried in an air atmosphere at 120°C to remove organic residuals. The powder was calcined in a small batch (2 g) in a silica crucible at 700°C in an air atmosphere for 1h to obtain the pure phase of BTO material.

2.2. Fabrication of Bi-Non Stoichiometric $\text{Bi}_4\text{Ti}_3\text{O}_{12}$ Material

The transmission electron microscope specimens were prepared by dispersing the synthesized material in ethanol subsequently sonicated briefly and dipped over a carbon-film copper grid and placed into the HRTEM. The average size of the particles is about 250 nm (which is used in this study).

The sample was allowed to expose in e-beam and the formation of the Bi-non-stoichiometric $\text{Bi}_4\text{Ti}_3\text{O}_{12}$ nanomaterial (hereafter NBTO refers Non-stoichiometric BTO) was studied. The BTO nanoparticles were exposed to the electron beam with the current density ($J = 2.02 \times 10^7 \text{ A/m}^2$). The size of Bi nanoparticles ranges from 6 nm to 30 nm which is observed throughout this study. These experiments were repeated several times to affirm the fabrication process can be reproducible. The beam parameters are tabulated in Table 1.

Table 1. Electron beam parameters of the fabrication process.

S. No	Particulars	Value
1	Beam current	39.7 nA
2	Beam diameter	50 nm
3	Current density	$2.02 \times 10^7 \text{ A/m}^2$

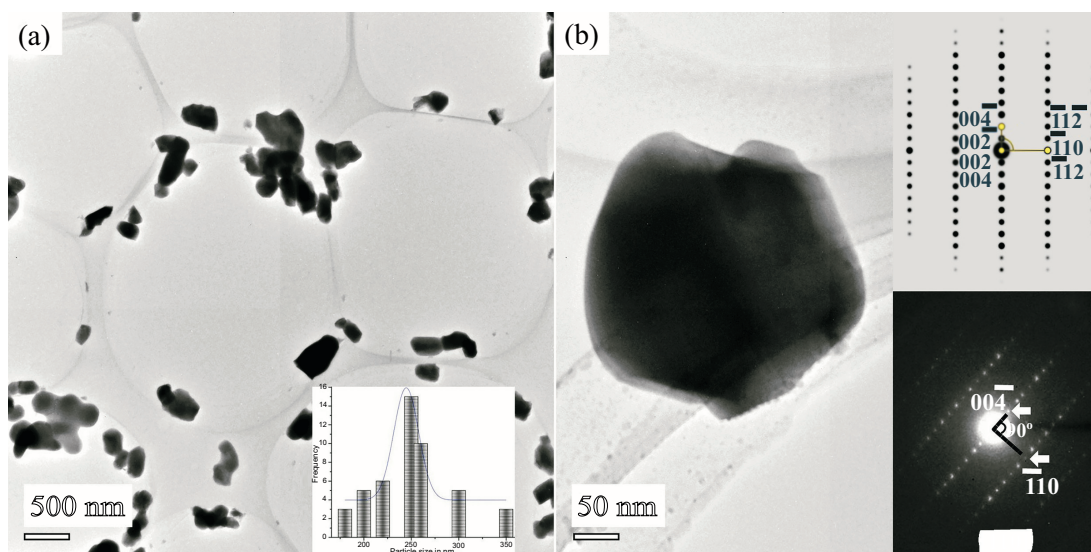


Fig. (2). TEM images of the $\text{Bi}_4\text{Ti}_3\text{O}_{12}$ particles. (a) A low magnification image which shows the morphology and particles distribution curve (inset). (b) A zoomed-in image of a single particle and the below and above insets are its corresponding SAED pattern and simulated diffraction pattern, respectively.

2.3. Characterization Techniques

The High Resolution Transmission Electron Microscopy (HRTEM), X-ray Energy Dispersive Spectroscopy (EDS) analysis and electron irradiation were performed in FEI Tecnai G^2 F30 microscope in which an electron beam produced by the field emission gun, operated at 300 kV. X-ray photoelectron spectroscopy (XPS) using a Thermo Electron Corporation ESCA Lab250 spectrometer at 15 kV and 150 W was employed to study the surface characteristics of irradiated and non-irradiated samples.

3. RESULTS AND DISCUSSIONS

3.1. Crystal Structure and Morphology of BTO Microparticles

We carried out Transmission Electron Microscopy (TEM) technique to acquire more information about the structural and the morphology of the synthesized material. Fig. (2a) shows the low magnification TEM image of the as-synthesized sample. It is found that most particles are polyhedral shapes with their sizes of about 180-300 nm. Due to the high calcination temperature treatment (essential to be a particle size more than 150 nm for this study) few particles are found to be clustered in a chain owing to the agglomeration of the particles. The mean particle size is calculated as 250 nm (the inset shows the particle size distribution graph). Fig. (2b) displays an individual BTO particle whose size is about 260 nm and the below inset is the corresponding Selected Area Electron Diffraction pattern (SAED) of the single particle (Recorded on the upper half of the particle). It confirmed that the crystalline BTO is presented in the synthesized sample. The reflection spots indicated by the arrows can be well indexed to $(00\bar{4})$, $(\bar{1}10)$ and $(\bar{1}12)$ planes. The above inset image is a simulated single crystalline diffraction pattern (zone axis $[110]$); both are consistent with each other. We found that the microparticle exhibits $Cmc2_1$ space group

structure of orthorhombic BTO. The extinction of $(00l)$ reflections, where l is odd, is resulted from the screw axis of 2_1 along $[001]$ direction. These results validate the statement; the synthesized material is BTO microparticles which has an orthorhombic crystal structure. To be skeptical about the purity of the synthesized BTO material, deliberately we examined the nano-scale structure of the various BTO particles on the surfaces and the edges (Fig. S1). (See Supplementary Information).

3.2. Crystal Structure and Morphology of Bi-NBTO

To fabricate the Bi-NBTO nanostructure, we illuminate BTO microparticle by e-beam in HRTEM. The Bi metal nanocrystals are formed at the perimeter of the BTO microparticle while the electron bombardment occurs in the target material. We found that the pure Bi metallic nanocrystals supported on NBTO microparticle could be synthesized by the electron beam irradiation at micro-scale level by the same e-beam parameters of our previous study [10]. The coexistence of the Bi metal nanocrystal, $\text{Bi}_4\text{Ti}_3\text{O}_{12-y}$ and $\text{Bi}_4\text{Ti}_3\text{O}_{12}$ composite has a great attention to investigate its unique physicochemical properties. Moreover, the non-illuminated part in the same Bi-NBTO structure furnishes a new class of *metal-n-type semiconductor-ferroelectric* smart material. This kind of novel material provides the new corridor to the emerging technologies. We utilized various precursor BTO particles for the sake of the reliability of this investigation and illustrated the corresponding HRTEM images in Fig. (3). We observed Bi nanocrystals are embedded in the non-stoichiometric BTO microparticles. Fig. (3a and b) are the same illuminated area at the initial time (after 30 seconds of illumination) and prolonged time (120 seconds of illumination), respectively. The white circle in the Fig. (3a) indicates the area of the e-beam. We can clearly notice that the small Bi nanocrystals emerge at the initial time of irradiation, whereas the

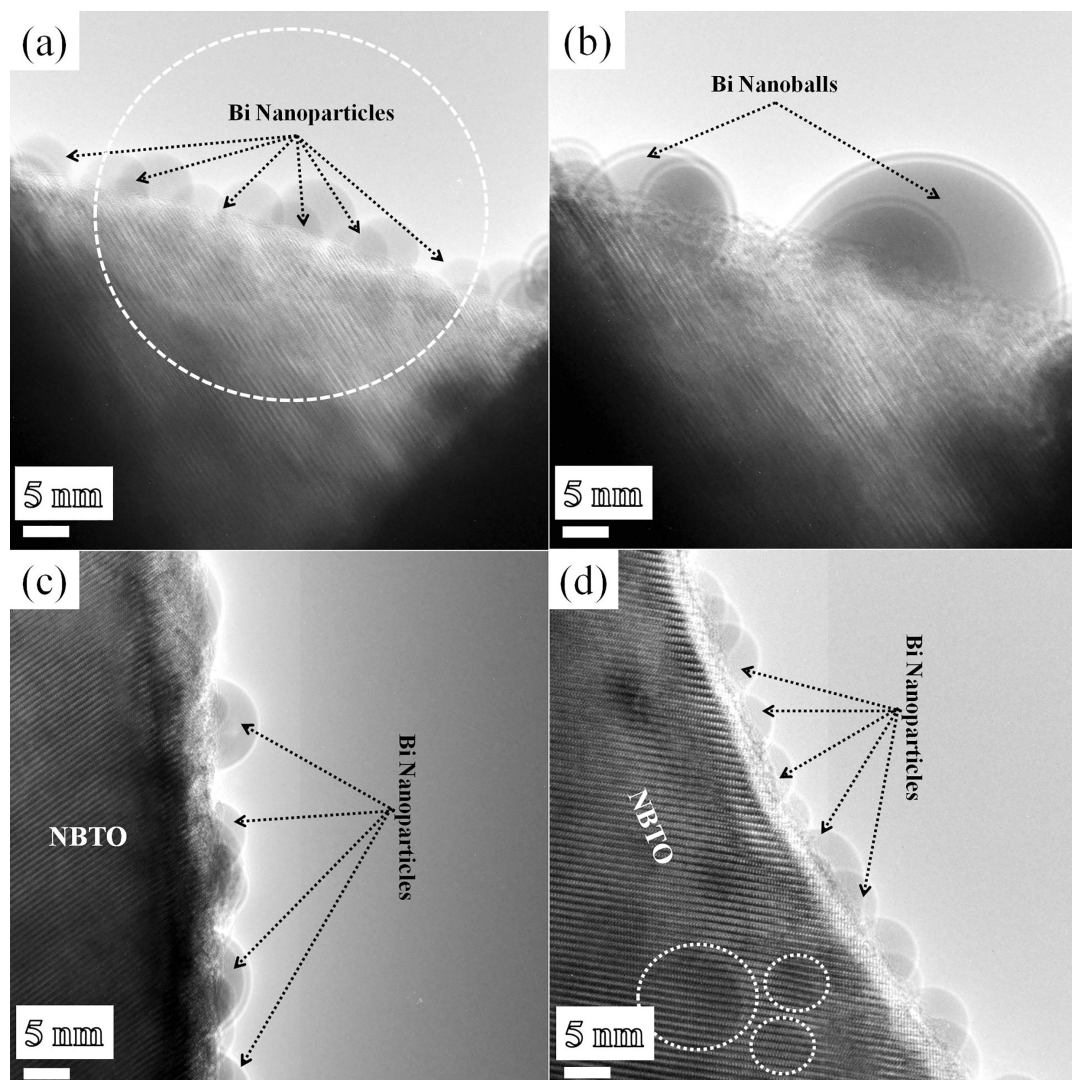


Fig. (3). (a) and (b) High resolution images of the same illuminated area at the initial time (30 sec) and prolonged time (120 sec) respectively. The white circle in the Fig. (3a) indicates the area of the e-beam. (c) and (d) are high resolution images of two different BTO precursor particles. The white circles in (d) indicate few Bi nanoparticles embedded in the BTO matrix.

irradiation time increases the nanocrystals coagulate into bigger particles. This can be explained by the following process. The formation of the bismuth nanoclusters/crystals occurred during the early minutes of irradiation. Once formed, these nanoparticles acted as seeds and grew into crystals. Some of these particles were able to grow into large crystals by the Ostwald ripening process. Sepulveda-Guzman *et al.* discovered the same phenomenon in the study of NaBiO_3 e-beam interaction [23]. To check the reliability of the Bi-NBTO formation, we randomly choose various BTO particles and continue the fabrication process. Fig. (3c and d) shows two different illuminated BTO particle, The evolution of Bi nanoparticle from the BTO leads to form NBTO followed by structural changes during the irradiation process. As a result, we observed the lattice distortion in the structural analysis. The small circles in Fig. (3d) indicate the Bi nanocrystals embedded in the BTO particles. Fig. (S2) (See Supplementary Information) shows morphology of the entire BTO particles after the prolonged Electro Beam Irradiation

(EBI) process. It displays fuzzy or cloudy like appearance due to the Bi nanoparticles are embedded in the BTO matrix.

To shed more light on the structure of the Bi and BTO particles, we carried out HRTEM analysis of the desired area. Fig. (4a) illustrates the high resolution TEM image of the Bi nanoparticle supported in the BTO particle. The size of the particle is 14 nm. The inset-1 is the corresponding FFT pattern of the selected area denoted as a white rectangle. The bright spots indicated can be indexed as the (020) and (200) planes of monoclinic Bi which belong to the space group of $C2/m$ (No. 12) viewed along the [001] zone axis, which has the following lattice parameters of $a = 6.674 \text{ \AA}$, $b = 6.117 \text{ \AA}$, $c = 3.304 \text{ \AA}$ and $\beta = 110.3^\circ$. The inset-2 is the simulated electron diffraction pattern. Both patterns are highly consistent with each other. In Fig. (4b) the layered NBTO structures are again clearly observed with small Bi nanoparticles. To affirm that the pure metallic Bi is present in the structure, we analyzed each emerged nanocrystal looking for the bismuth

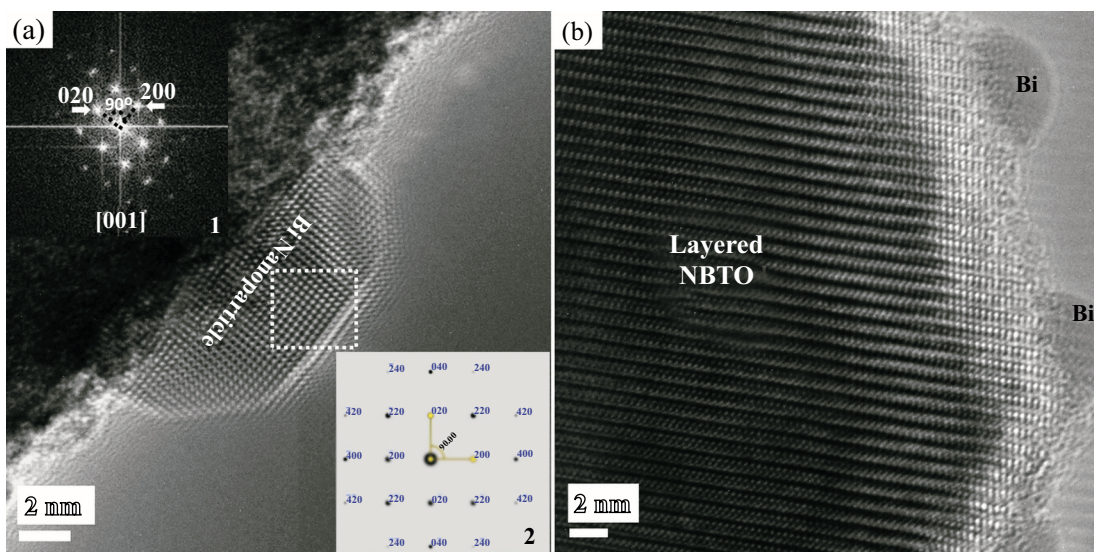


Fig. (4). High resolution images of Bi and BTO particles. (a) Bi-nanoparticle, inset-1 is corresponding FFT pattern of the selected area and inset-2 is simulated electron diffraction pattern. (b) Layered NBTO microparticle along with Bi nanoparticle.

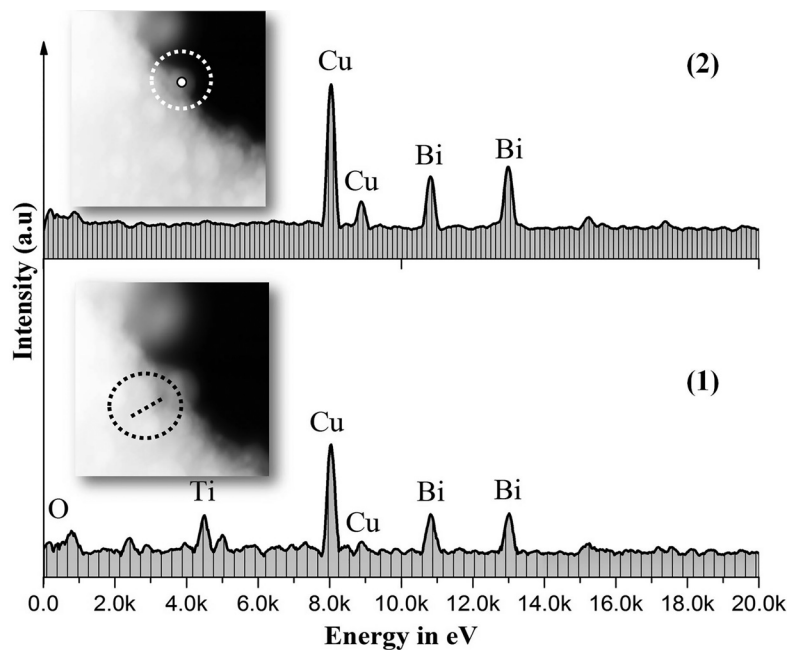


Fig. (5). EDS spectra of the BTO material after irradiation. (1) and (2) are the spectra obtained from the scanned area as shown in the inset NBTO and Bi, respectively.

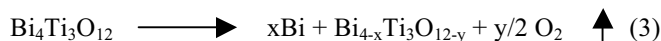
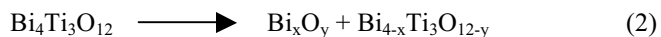
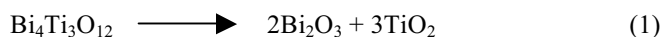
oxide species like BiO, Bi₂O₃, Bi₂O₄ and etc but we did not find any other species than the Bi metal. This result argues that the obtained nanocrystals are pure Bi metal along with NBTO. Usually, most of the previous works state that the rhombohedral and cubic Bi were obtained in both the wet chemical synthesizes [24] and the e-beam irradiation [23]. Oshima *et al.* [25] observed a transition from rhombohedral to the cubic structure in 6-7 nm diameter Bi particles under an electron beam; however, in our case, the monoclinic Bi obtained in 14 nm size particle.

3.3. The Chemical Composition of Bi-NBTO

We employed the Energy Dispersive Spectroscopy (EDS) method at different stages during the irradiation process in

order to study the changes in chemical composition of the material. Fig. (5) depicts the typical EDS spectrum at different levels of radiation. After the irradiation process, the acquired spectrum shows Bi, Ti and O peaks (inclusive of Cu and C peaks which belong to the sample grid). In Fig. (5) (1) and (2) are the BTO and Bi particle EDS spectrum, respectively. The line profile scanned area shown in the inset for BTO in the spectrum (1). The single spot scanned area shown in the inset for Bi in the spectrum (2). To be skeptical of BiO evolution from the BTO matrix, we deliberately analyzed a newly emerged particle on the surface of the BTO matrix. The EDS spectrum shows that only Bi-element presents at 99%. Moreover, the reduction of oxygen around 10 to 20% is observed in the spectrum (1). The semi-

quantitative analysis was consistent with the atomic composition of the NBTO and Bi. It is well known that the $\text{Bi}_4\text{Ti}_3\text{O}_{12}$ particles will decompose while irradiated with the electron beam. It can be explained by the following three possible mechanisms:



We did not observe any bismuth oxide and titanium oxide species during this study. If the formation mechanism complies with Eq. 1 and 2, the semi-quantification EDS analysis must show the total at. % of Bi, Ti and O in the scanned region, which is either equal to $\text{Bi}_4\text{Ti}_3\text{O}_{12}$ or increase in Bi and O, but there is no evidence of such bismuth / titanium oxide with $\text{Bi}_{4-x}\text{Ti}_3\text{O}_{12-y}$ formation. These results exhibited that Eqs. 1 and 2 are not a promising mechanism. Considering Eq. 3; after the irradiation of the BTO particle, the final products are Bi, $\text{Bi}_{4-x}\text{Ti}_3\text{O}_{12-y}$ and oxygen which enters into the vacuum as a gas, which is consistent with the EDS spectrum as well as structural analysis results. The deprivation of oxygen in the vacuum can be explained by an electron-stimulated desorption process. On the whole, the third mechanism is a possible way to explain the formation of pure Bi supported in the cation deficient BTO matrix.

3.4. Electronic and Surface Characteristics of BTO and Bi-NBTO

Electronic band structures and surface characteristics of non-irradiated and irradiated BTO materials were studied by X-ray Photoelectron Spectroscopy (XPS) method and Gaussian fitting. Figs. (6 a-f) illustrate the typical XPS spectra. It can be seen that the materials consist of Bi, Ti and O elements. Figs. (6a, c and e) show narrow scan XPS spectra of Bi 4f, Ti 2p and O 1s, respectively, of a non-irradiated BTO sample. The Bi 4f spectra can be deconvoluted into two major components Bi $4f_{7/2}$ and Bi $4f_{5/2}$ as observed in Fig. (6a). The major peaks at 158.7 and 163.9 eV are attributed to the Bi lattice in BTO crystal. Ti 2p deconvoluted spectrum shows only one spin-orbit doublet as shown in Fig. (6c). The first component around 458.2 eV is attributed to the Ti $2p_{3/2}$ peak, whereas the second one around 464.7 eV is attributed to Ti $2p_{1/2}$ peak of Ti^{4+} . The O 1s spectrum can be deconvoluted into two components as shown in Fig. (6e). The minor peak at higher binding energy (530.8 eV) is assigned to the adsorbed oxygen; the major component at low binding energy (529.7 eV) is assigned to lattice oxygen in the BTO. All assigned peak values are well matched with the previously reported work [26]. Figs. (6b, d and f) show core-level XPS spectra of Bi 4f, Ti 2p and O 1s, respectively, of an irradiated BTO sample. The irradiated sample exhibits considerable changes in its surface characteristic with its counterpart non-irradiated BTO. It is clearly seen that Bi 4f doublet exhibits two Bi $4f_{7/2}$ components at 156.6 eV and 158.7 eV. The lower binding energy components at 156.6 eV is assigned to the Bi metal of Bi^0 . The surface characteristic study reveals the

Bi metal co-exists with the non-stoichiometric BTO. As we discussed earlier, the Bi metal formed by the reduction of Bi^{3+} ions to Bi^0 . We did not notice any substantial deviation between the Ti 2p and the O 1s spectra of non-irradiated and irradiated BTO samples as indicated in Fig. (6d and f).

It is well known that the band structure of materials can be altered by external stimuli. The new electronic state was obtained in the irradiated BTO particles as a result of Bi-NBTO structures. Fig. (7a) shows valence band spectrum of the non-irradiated and irradiated BTO. For the non-irradiated BTO, The band A region consists basically of O 2p states hybridized with Bi 6s, Bi 6p and Ti 3d states and this region is the evidence for the Bi-O-Ti bonding interaction. The band B region is assigned to mainly Bi-O bonding interaction. The intensity of the B region reduces due to the diminishment of the Bi-O bond interaction. These results are consistent with the reported value [27]. As shown in Fig. (7a), by taking the baseline intercept of a linear fit to the valence band edge, the Valence Band Maximum (VBM) energy positions in the non-irradiated and irradiated BTO were determined to be 1.45 ± 0.1 eV and 1.8 ± 0.1 eV, respectively. The change in VBM position can be understood by the theory of metal-semiconductor contact. Before the irradiation, the VBM of the BTO microparticle is 1.45 ± 0.1 eV, which indicates that the BTO microparticle is close to an intrinsic semiconductor (the band gap of BTO is 2.9~3.1 eV) [28]. After irradiation, the newly formed metallic Bi nanoparticles contact with BTO nanoparticle, changing the Fermi level and thus VBM. As a result, the irradiated BTO nanoparticle becomes n-type. Fen Liu *et al.* reported that Schottky barrier height of various metals with BTO, which stated that the metal contact influences the Fermi level pinning [29]. In our case, the Bi metal influences the Fermi level of the ferroelectric BTO.

3.5. Formation Mechanism and Future Applications

The absolute mechanism of the formation of Bi-NBTO by electron-beam irradiation is still not entirely understood. However, in our case, the electrostatic charging is created in the specimen as soon as the precursor is exposed to the high EBI due to its insulating nature. Consequently, the electric field increases in a high level at the edge of the illuminated area due to poor conductivity of the BTO microparticle. This leads to the ejection of the metallic Bi atom from the precursor. Initially, no Bi crystals are observed; at a critical time Bi nanocrystals are emerged. Newly emerged Bi atoms were then deposited on the supporting NBTO nanoparticle, forming nanoparticle in a few nanometers with different morphologies as shown in Figs. (3 and 4). The outcome of *in situ* HRTEM study furnishes the formation, growth and coagulation of Bi nanocrystals. An earlier study proved that the electron-stimulated desorption occurs in perovskite transition-metal oxides *via* Knotek-Feibelman (KF) mechanism [10]. We believe that the formation of Bi-NBTO may also follow the KF mechanism. The core hole / inner-shell vacancy created on the metal ion (Bi^{3+}) by the incident electron is followed by (interatomic) Auger decay from the oxygen. This consequence in a neutral or positive O atom by

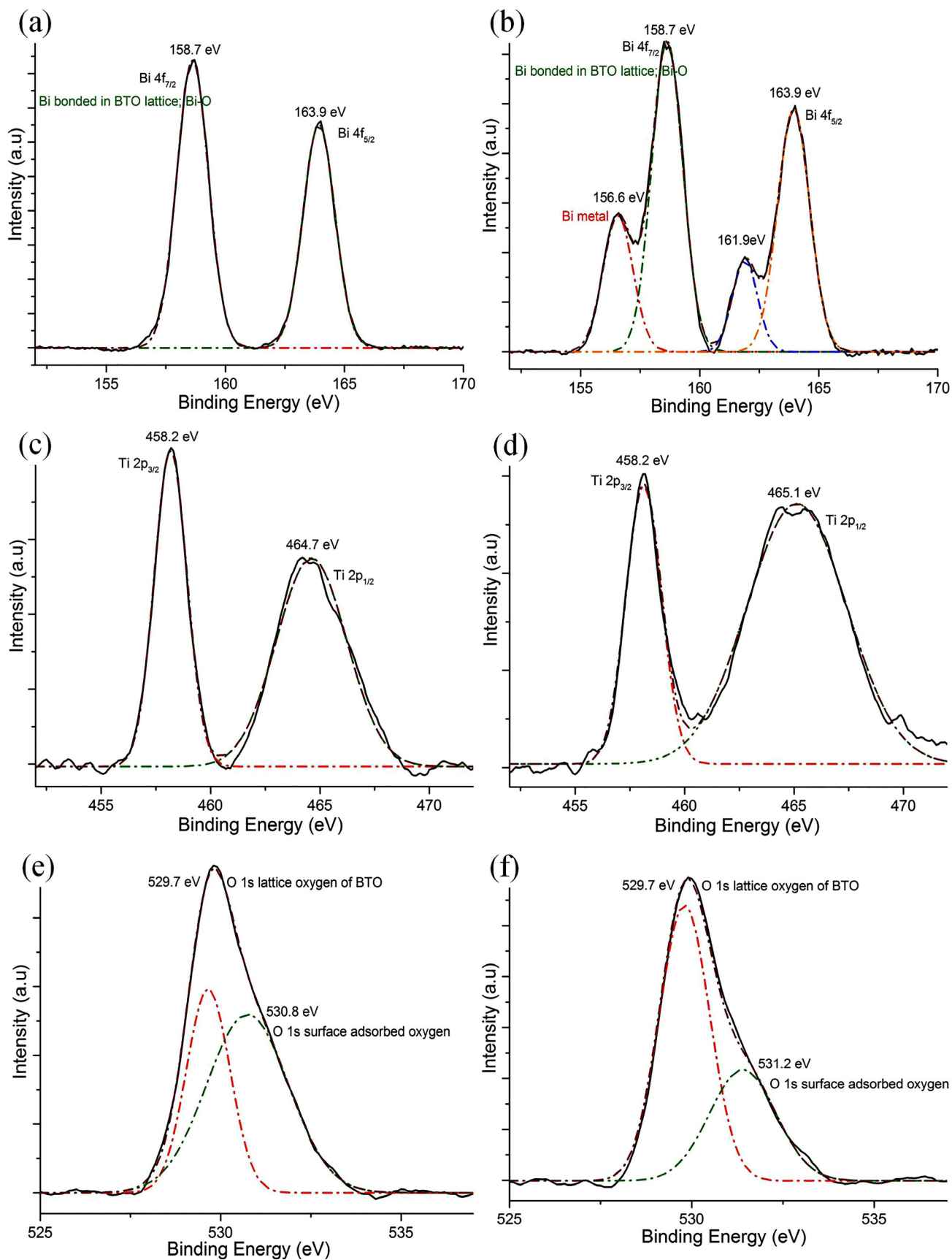


Fig. (6). (a, c and e) XPS spectra of non-irradiated BTO nanoparticle. (b, d and f) XPS Spectra of an irradiated BTO nanoparticle. From top to bottom core level spectra of Bi 4f, Ti 2p and O 1s are plotted with deconvoluted spectra.

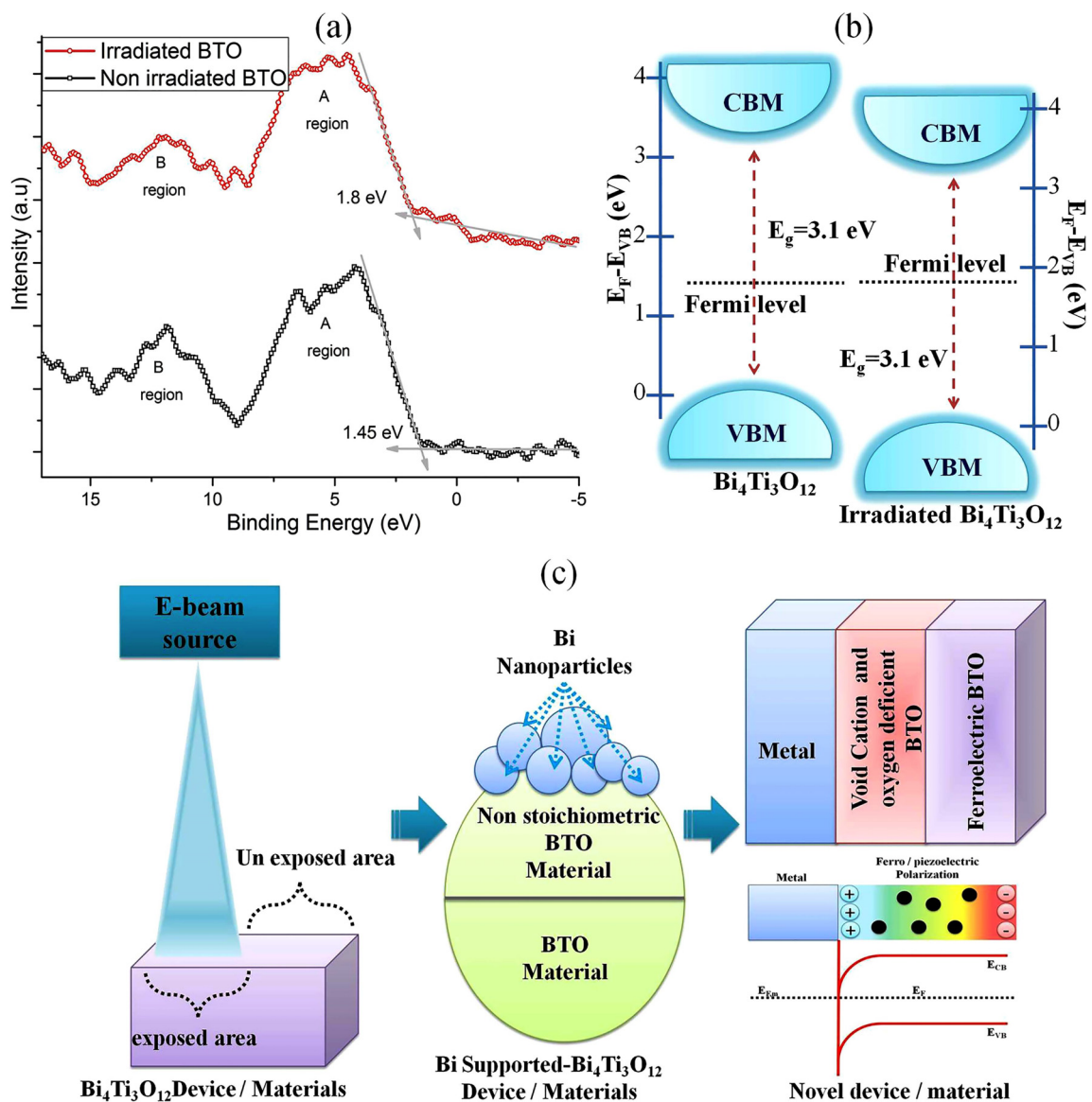
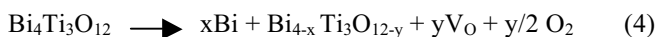


Fig. (7). (a) Valence band spectra of non-irradiated and irradiated BTO microparticle. (b) Band alignment structure of the non-irradiated BTO and irradiated BTO. (c) Schematic illustration of the fabrication process to obtain novel functional/smart materials.

a simple Auger process involves the loss of two electrons (one to fill the core hole on the cation and second emitted as an Auger electron, resulting in O^{2-} ion converted to an O atom). Sometimes the two Auger electrons emitted and O^+ ion will be formed which is repelled by Coulomb interaction with the surrounding Bi^{3+} metal ions and stripped out from the surface.



A more elaborated study of Bi-NBTO-BTO formation is required; nevertheless, the synthesis of $x\text{Bi}-\text{Bi}_{4-x}\text{Ti}_3\text{O}_{12-y}-\text{Bi}_4\text{Ti}_3\text{O}_{12}$ nanostructure under e-beam is highly interesting for nano/microelectronics purposes. Badapanda *et al.* discovered that the A-site deficient cation BaTiO_3 is a good candidate for the relaxor application [21]. Our synthesized

material consists of metal, (n-type semiconductor) A-site deficient relaxor BTO and ferroelectric (or p-type semiconductor) BTO, which possess the unique features and it is a new class of material with multi-functionality as shown in Fig. (7c). The entire process of the fabrication method is illustrated in this figure.

CONCLUSION

A new class of multifunctional material like metal-n-type semiconductor/ferroelectric (Bi-NBTO-BTO) is synthesized at a micro-scale level in HRTEM and investigated systematically. Furthermore, the electronic structure and surface features were studied extensively by the XPS technique. This state that the intrinsic semiconductor property can be changed by e-beam and one can construct the p-n junction. This study offers the pathway to the materials scientist to explore the physicochemical properties

of the new generation smart materials. Moreover, this study proves that one can engineer the desired materials and study their characteristics in real-time mode at HRTEM on a micro-scale level too.

CONSENT FOR PUBLICATION

Not applicable.

CONFLICT OF INTEREST

The authors declare no conflict of interest, financial or otherwise.

ACKNOWLEDGEMENTS

This work is supported by the National Natural Science Foundation of China (No. 51231007, 51571197, 51501194, 51671194, 51521091, and 51401212), National Basic Research Program of China (2014CB921002), and Chinese Academy of Sciences (QYZDJ-SSW-JSC010). J. S. acknowledges the IMR-CAS Doctoral Fellowship. The authors are grateful to B. Wu and L. X. Yang of this laboratory for their technical support on the Titan platform of G2 60-300kV aberration-corrected scanning transmission electron microscope.

SUPPLEMENTARY MATERIAL

Supplementary material is available on the publisher's website along with the published article.

REFERENCES

- [1] Drossel, W.G.; Kunze, H.; Bartón, D.H.; Bucht, A.; Weisheit, L.; Pagel, K. Smart³-Smart materials for smart applications. *Procedia CIRP*, **2015**, *36*, 211-216.
- [2] Kamila, S. Introduction, classification and applications of smart materials. *Am. J. Appl. Sci.*, **2013**, *10*(8), 876-880.
- [3] Tzou, H.S.; Lee, H.J.; Arnold, S.M. Smart materials, precision sensors/actuators, smart structures and structronic systems. *Mech. Adv. Mater. Structures*, **2004**, *11*(4-5), 373-393.
- [4] Chu, L.Y.; Xie, R.; Ju, X.J.; Wang, W. *Smart Hydrogel Functional Materials*, 1st ed; Springer: Germany, **2012**.
- [5] Anderson, D.G.; Burdick, J.A.; Langer, R. Materials science. Smart biomaterials. *Science*, **2004**, *305*(5692), 1923-1924.
- [6] Khan, A.; Abas, Z.; Kim, H.S.; Oh, K. Piezoelectric thin films: An integrated review of transducers and energy harvesting. *Smart Mater. Struct.*, **2016**, *25*, 053002-053018.
- [7] Heyderman, L.J.; Stamps, R.L. Artificial ferroic systems: Novel functionality from structure, interactions and dynamics. *J. Phys. Condens. Matter*, **2013**, *25*(36), 363201-363230.
- [8] Agar, J.C.; Pandya, S.; Xu, R.J.; Yadav, A.K.; Liu, Z.Q.; Angesten, T.; Saremi, S.; Asta, M.; Ramesh, R.; Martin, L.W. Frontiers in strain-engineered multifunctional ferroic materials. *MRS Commun.*, **2016**, *6*, 151-166.
- [9] Gonzalez-Martinez, I.G.; Bachmatiuk, A.; Bezugly, V.; Kunstmann, J.; Gemming, T.; Liu, Z.; Cuniberti, G.; Rümmeli, M.H. Electron-beam induced synthesis of nanostructures: A review. *Nanoscale*, **2016**, *8*(22), 11340-11362.
- [10] Suriyaprakash, J.; Xu, Y.B.; Zhu, Y.L.; Yang, L.X.; Tang, Y.L.; Wang, Y.J.; Li, S.; Ma, X.L. Designing of metallic nanocrystals embedded in non-stoichiometric perovskite nanomaterial and its surface-electronic characteristics. *Sci. Rep.*, **2017**, *7*(1), 8343.
- [11] Murakami, S. Quantum spin Hall effect and enhanced magnetic response by spin-orbit coupling. *Phys. Rev. Lett.*, **2006**, *97*(23), 236805.
- [12] Smith, G.E.; Baraff, G.A.; Rowell, J.M. Effective g factor of electrons and holes in bismuth. *Phys. Rev.*, **1964**, *135*, A1118.
- [13] Tang, C.J.; Li, G.H.; Dou, X.C.; Zhang, Y.X.; Li, L. Thermal expansion behaviours of bismuth nanowires. *J. Phys. Chem. C*, **2009**, *113*, 5422-5427.
- [14] Arias, D.V.; Dube, I.Z.; Diaz, D.; Jacinto, P.S.; Ruiz Ruiz, V.F.; Castillo Blum, S.E.; Rendon, L. Stabilization of strong quantum confined colloidal bismuth nanoparticles, one pot synthesized at room conditions. *J. Phys. Chem. C*, **2012**, *116*, 14717-14727.
- [15] Jardiel, T.; Caballero, A.C.; Villegas, M. Aurivillius ceramics: Bi₄Ti₃O₁₂ based piezoelectrics. *J. Ceram. Soc. Jpn.*, **2008**, *116*, 511-518.
- [16] Cummins, S.E. Ferroelectric domains in Bi₄Ti₃O₁₂ single crystals. *J. Appl. Phys.*, **1966**, *37*, 2510.
- [17] Zhou, Q.Z.; Kennedy, B.J. Structural studies of the ferroelectric phase transition in Bi₄Ti₃O₁₂. *Chem. Mater.*, **2003**, *15*, 5025-5028.
- [18] Nakamura, T.; Muhammet, R.; Shimizu, M.; Shiosaki, T. Preparation of Bi₄Ti₃O₁₂ films by MOCVD and their applications to memory devices. *Integr. Ferroelectr.*, **1995**, *6*, 35-46.
- [19] Zhang, F.Q.; Li, Y.X. Recent progress on bismuth layer structured ferroelectrics. *J. Inorg. Mater.*, **2014**, *6*(5), 449-460.
- [20] Yao, F.Y.; Xu, X.H.; Wang, H.; Zhou, J.T.; Yang, X.N.; Zhang, Y.; Shang, S.X.; Huang, B.B. Photocatalytic property of perovskite bismuth titanate. *Appl. Catal. B*, **2004**, *52*, 109-116.
- [21] Bandapanda, T.; Senthil, V.; Rana, D.K.; Panigrahi, S.; Anwar, S. Relaxor ferroelectric behaviour of "A" site deficient bismuth doped barium titanate. *J. Electroceram.*, **2012**, *29*, 117-124.
- [22] Long, C.; Chang, Q.; Fan, H. Differences in nature of electrical conduction among Bi₄Ti₃O₁₂-based ferroelectric polycrystalline ceramics. *Sci. Rep.*, **2017**, *7*(1), 4193.
- [23] Guzman, S.S.; Villarreal, N.E.; Ferrer, D.; Castro, A.T.; Zhou, J.P.; Yacamán, M.J. *In situ* formation of bismuth nanoparticles through e-beam irradiation in a transmission electron microscope. *Nanotechnology*, **2007**, *18*, 335604.
- [24] Wang, F.D.; Tand, R.; Heng, Y.; Gibbons, P.C.; William, E.B. Size and shape controlled synthesis of bismuth nanoparticles. *Chem. Mater.*, **2008**, *20*, 3656-3662.
- [25] Oshima, Y.; Takayanagi, K.; Hirayama, H. Structural anomaly of fine bismuth particles observed by ultra high-vacuum TEM. *Z. Phys. D.*, **1997**, *40*, 534-538.
- [26] Li, S.P.; Bian, X.B.; Gao, J.Z.; Zhu, G.Q.; Hojamberdiev, M.; Wang, C.H.; Wei, X.M. Effect of oxygen vacancy and surface Plasmon resonance: A photocatalytic activity study on Ag/Bi₄Ti₃O₁₂ nanocomposites. *J. Mater. Sci. Mater. Electron.*, **2017**, *28*, 7731.
- [27] Postnikov, A.V.; Bartkowski, S.; Mersch, F.; Neumann, M.; Kurmaev, E.Z.; Cherkashenko, V.M.; Nemnonov, S.N.; Galakhov, V.R. Electronic structure and valence-band spectra of Bi₄Ti₃O₁₂. *Phys. Rev. B Condens. Matter*, **1995**, *52*(16), 11805-11812.
- [28] Hou, D.; Hu, X.; Hu, P.; Zhang, W.; Zhang, M.; Huang, Y. Bi₄Ti₃O₁₂ nanofibers-BiOI nanosheets p-n junction: Facile synthesis and enhanced visible-light photocatalytic activity. *Nanoscale*, **2013**, *5*(20), 9764-9772.
- [29] Liu, F.; Ma, Y.; Yang, F.; Zhou, Y.C. Schottky barrier height and conduction mechanism in ferroelectric bismuth titanate. *Appl. Phys. Lett.*, **2010**, *96*, 52102.